The structure and antigenicity of a type C foot-and-mouth disease virus

S Lea[1‡], J Hernández[2‡], W Blakemore[3], E Brocchi[4], S Curry[3†], E Domingo[2], E Fry[1], R Abu-Ghazaleh[3], A King[3], J Newman[3], D Stuart[1,5*] and MG Mateu[2]

[1]Lab. of Molecular Biophysics, Rex Richards Building, University of Oxford, South Parks Road, Oxford, OX1 3QU, UK, [2]Centro de Biología Molecular "Severo Ochoa" (CSIC-UAM), Universidad Autónoma de Madrid, Cantoblanco, 28049 Madrid, Spain, [3]Institute for Animal Health, Ash Road, Pirbright, Woking GU24 0NF, UK, [4]Istituto Zooprofilattico Sperimentale della Lombardia e dell'Emilia, 25125 Brescia, Italy and [5]Oxford Centre for Molecular Sciences, New Chemistry Laboratory, Oxford OX1 3QT, UK

Background: Picornaviruses are responsible for a wide range of mammalian diseases and, in common with other RNA viruses, show considerable antigenic variation. Foot-and-mouth disease viruses (FMDVs) constitute one genus of the picornavirus family and are classified into seven serotypes, each of which shows considerable intratypic variation. This antigenic variation leads to continuing difficulties in controlling the disease. To date the structure of only one serotype, O, has been reported.
Results: The three-dimensional structure of a serotype C (isolate C-S8c1) FMDV, has been determined crystallographically at 3.5 Å resolution. The main chain conformation of the virion is very similar to that of type O_1 virus. The immunodominant G–H loop of VP1, the presumed site of cell attachment, is disordered in both types of virus indicating a functional role for flexibility of this region. There are significant changes in the structure of other antigenic loops, and in some internal regions involved in protomer–protomer contacts, including the entire amino-terminal portion of VP2, described here for the first time for a picornavirus. Antigenic sites have been identified by genetic and peptide mapping methods, and located on the capsid. The data reveal a major new discontinuous antigenic site (site *D*) which is located near to the three-fold axis and involves residues of VP1, VP2 and VP3 which lie adjacent to each other on the capsid.
Conclusion: In FMDV type C, amino acid substitutions seen in mutants that are resistant to neutralization by monoclonal antibodies (MAbs) map to predominantly surface-oriented residues with solvent-accessible side-chains not involved in interactions with other amino acids, whereas residues which are accessible but not substituted are found to be more frequently involved in protein–protein interactions. This provides a molecular interpretation for the repeated isolation of the same amino acid substitutions in MAb-resistant variants, an observation frequently made with RNA viruses. This first comparison of two FMDV serotypes shows how subtle changes at antigenic sites are sufficient to cause large changes in antigenic specificity between serotypes.

Structure 15 February 1994, **2**:123–139

Key words: antigenicity, foot-and-mouth disease virus, macromolecular crystallography, virus structure

Introduction

The determination of high-resolution, three-dimensional structures of whole viruses by X-ray crystallography enables fuller interpretations of biological properties, including antigenicity. To date the best studied viruses have been the picornaviruses which, due to their relatively small size (diameter ~300 Å, M_r ~8 MDa) and unenveloped nature, are particularly amenable to crystallographic analysis. The structures of several picornaviruses have now been determined including those of two serotypes of poliovirus [1,2], three serotypes of rhinovirus [3–5], mengovirus [6], two types of Theiler's murine encephalomyelitis virus [7,8] and foot-and-mouth disease virus (FMDV) isolate O_1BFS [9]. These structures reveal many striking similarities and differences within this viral family. The capsids of all these picornaviruses are found to consist of 60 copies each of four proteins: VP1–4. VP1, VP2 and VP3 are structurally similar to one another and have at their core an eight-stranded β-sandwich, composed of two four-stranded β-sheets, the strands of which are conventionally labelled alphabetically, according to their order in the amino acid sequence, namely CHEF and BIDG respectively. Loops connecting the strands are identified by the strands they join. These surface-exposed loops are implicated in viral antigenicity. VP4 is smaller and confined to the capsid interior.

The molecular changes underlying the antigenic diversification of viruses must preserve a functional capsid. Not only must the virion remain stable but it must also retain the ability to infect susceptible cells by binding to a cellular receptor, whilst escaping immune detection. This imposes conflicting demands on the capsid surface. In enteroviruses, rhinoviruses and cardioviruses it is thought that receptor-binding residues enjoy a protected location in a narrow cleft or pit inaccessible

*Corresponding author. †Present address: Dept. of Biological Chemistry, Harvard MedicalSchool, 240 Longwood Avenue, Boston MA 02115, USA. ‡SL and JH have contributed equally to this work

to antibodies. This hypothesis has been most clearly demonstrated for the major receptor group of rhinoviruses [10,11], in which these surface depressions form a continuous 'canyon' around the five-fold axis. FMDV, however, has a comparatively smooth surface, with no canyon in which receptor binding residues may be concealed. In the case of FMDV, attachment to the cell receptor is mediated by a conserved RGD (Arg–Gly–Asp) sequence [12] which, in complete contrast to these other picornaviruses, is located at the tip of a long exposed loop. Although this loop, the G–H loop of VP1, is accessible to antibodies (indeed it is strongly antigenic), it appears that variation in the sequences either side of the RGD serves to camouflage these vital residues from antibody attack [9].

The O_1BFS structure contained no model for the VP1 G–H loop as it was absent from the electron density map, an indication of a high degree of flexibility either internally or at particular hinge regions. Further studies showed that the conformation/orientation of this loop could be modified by point mutations elsewhere on the capsid surface [13] and suggested that a disulphide bond linking the loop to VP2 could be a key determinant of the loop conformation. The structure of type O_1 FMDV in which this disulphide bond has been broken (reduced O_1BFS) [14] shows the loop adopting a stable conformation lying over the surface of VP2. This disulphide bond, thus shown to be responsible for maintaining loop mobility of the native (i.e. oxidized) O_1 virus, is not present in the majority of FMDVs (it is characteristic of subtype O_1 viruses). To investigate whether flexibility and conformational variability of this loop are important in other FMDV serotypes we have undertaken X-ray crystallographic analyses of type A and type C viruses. Here we report the structure of isolate C-S8c1, a representative of the European C_1 subtype.

FMDV is highly varied antigenically, with each of the seven serotypes encompassing numerous poorly cross-protecting subtypes and variants. The determination of the type C crystal structure has provided an opportunity, for the first time, to make a detailed comparison of two FMDV serotypes, and thus to gain insights into the structural basis of serotype diversity. We have also complemented these structural studies by an analysis of the antigenicity of FMDV C-S8c1. Two antigenic sites have previously been identified in C-S8c1 FMDV using a combination of genetic and peptide mapping techniques [15]. In this paper we present a more complete study based on an enlarged panel of 31 monoclonal antibodies (MAbs), which has revealed a third, major antigenic site. The locations of antigenic residues are here interpreted in the light of our crystallographic data in order to provide a more detailed understanding of the mechanism of antigenic change, and of the structural constraints that limit such change.

Results and discussion

Structure determination

FMDV strain C-S8c1 was crystallized as previously described [16]. The crystals have the same morphology (rhombic dodecahedra) and space group (I23) as crystals of O_1BFS (although the unit cell is slightly expanded, a ~348 Å compared with 345 Å for O_1BFS), the crystallographic asymmetric unit is therefore 1/12 of a virus particle, being composed of five copies of each of the capsid proteins. Crystals grow to a maximum length of 0.4 mm in the longest dimension but are unstable, becoming opaque within 10 days. Degraded crystals show little or no diffraction.

X-ray diffraction data were collected on station 9.6 of the SERC SRS, Daresbury. The crystals rarely diffracted beyond Bragg spacings of 3.5 Å, the resolution limit for the structure determination. Radiation damage limited the crystal life-time to one or two exposures, examination of 52 crystals yielding 35 useful film packs. Post-refinement [17] showed the typical mosaic spread of the crystals to be 0.09°. Data processing statistics are shown in Table 1.

Table 1. Final data processing statistics for all C data sets.

Data set	R(I) all data (%)	No. of reflections Total	Independent	% Complete to 3.5 Å All data	Data I > 3σI
C-S8c1	18	98 942	64 849	74	50
SD6-6	18	64 779	52 664	60	37
'Master'	18		79 016	90	63

$R(I) = (\Sigma_h \Sigma_i | (I_h - I_{hi}) |) / (\Sigma_h \Sigma_i I_{hi}) \times 100$

Due to uncertainties in the X-ray wavelength, the size of the unit cell, relative to that of O_1BFS, was determined precisely using a grid search in X-PLOR [18] with a correctly oriented O_1BFS model as a search object (Fig. 1). This search yielded a clear minimum value for R_C at a = 347.6 Å, where:

$$R_C = \frac{\sum_h |(|F_{h,obs}| - |F_{h,calc}|)|}{\sum_h |F_{h,obs}|} \times 100$$

Structure factors generated using the O_1BFS model in this C-S8c1 cell, scaled to the observed structure factors for C-S8c1 with R_C = 31.1 %. A Wilson plot [19] indicated that the B-factors for the initial C-S8c1 model were, on average, 30 Å^2 higher than for the O_1BFS model. The phases calculated from this model were then refined against the C-S8c1 data using a standard procedure for five-fold real-space averaging and solvent flattening [20]. On convergence (40 cycles) the mean phase change from the starting phases was 39°. A $2|F_{obs}| - |F_{calc}|$ electron density map, calculated to 3.5 Å resolution, using these refined phases, was of surprisingly high quality (especially in the light of the rela-

tively poor ordering in these crystals). The amino acid substitutions between O_1BFS and C-S8c1 were clearly evident, indicating that there was no residual bias in the phases. A model with the correct C-S8c1 amino acid sequence was built into the map with little difficulty. Successive cycles of rebuilding and refinement of the model followed.

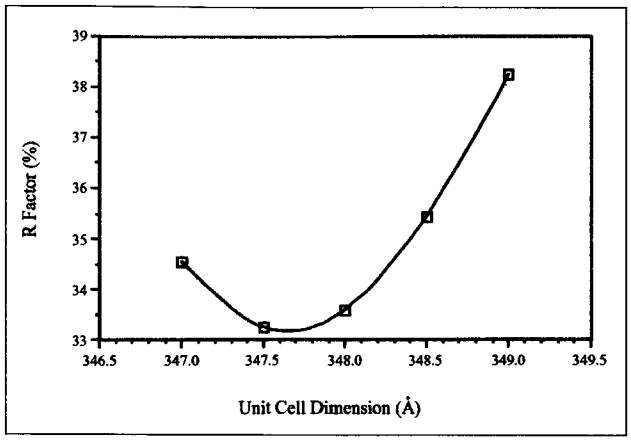

Fig. 1. A plot of R-factor for agreement between $|F_{calc}|$ generated by placing the O_1BFS coordinates in 123 unit cells of different dimensions and the $|F_{C\text{-}S8c1,\ obs}|$.

At this stage data from MAb-resistant (MAR) mutant SD6-6 [21] were collected. SD6-6 is a MAb SD6-resistant mutant of FMDV C-S8c1, with the single amino acid substitution in VP1, Ser139→Ile (C-S8c1 numbering: position 139 is equivalent to 143 in O_1BFS). A difference map calculated with coefficients $|F_{C\text{-}S8c1,\ obs}| - |F_{SD6\text{-}6,\ obs}|$ using the phases from cycle 40 of the real-space averaging revealed no peaks above background. Lack of any detectable conformational differences between SD6-6 and C-S8c1 suggested combination of the data sets to give a more complete C 'master' set would be valid (Table 1). Further cycles of real-space averaging were implemented with this 'master' data set. The final phases from the previous C-S8c1 averaging were taken as the start point for this averaging, which was performed using program GAP (J Grimes and D Stuart, unpublished program). Molecular envelopes were calculated at cycles 1 and 13 and the averaging converged after 30 cycles, at which point the agreement between the observed data and those calculated from back-transformation of the averaged map was excellent; R_{AV} = 11.86 % and C = 0.954 where:

$$R_{AV} = \frac{\sum_h |(|F_{h,obs}| - |F_{h,av}|)|}{\sum_h |F_{h,obs}|} \times 100$$

$$C = \frac{\sum_h (\overline{F}_{obs} - |F_{h,obs}|)(\overline{F}_{av} - |F_{h,av}|)}{\left[\sum_h (\overline{F}_{obs} - |F_{h,obs}|)^2 \cdot \sum_h (\overline{F}_{av} - |F_{h,av}|)^2\right]^{1/2}}$$

(Fig. 2). The mean phase change from the starting phases was 30° (37° from the phases from the O1BFS model). This map (Fig. 3) confirmed the original C-S8c1 maps, but gave improved clarity in some of the less well ordered regions. A difference map for the SD6-6 virus, calculated with these new phases confirmed the original result; no difference in the conformation of any of the capsid proteins (or internal features) can be seen between virus C-S8c1 and SD6-6. Minor rebuilding and a final round of positional and B-factor refinement using the combined 'master' data set gave R_C of 21 % for all data between 25–3.5 Å, with strict five-fold non-crystallographic constraints. This model contains 670 residues and has good stereochemistry (Table 2).

Structural differences between C-S8c1 and O_1BFS FMDV

C-S8c1 and O_1BFS share 82 % sequence identity in the four capsid proteins. As expected, the C-S8c1 structure is basically very similar (Fig. 4) to that previously described for O_1BFS [9]. The disposition of the proteins in the capsid is indistinguishable, as are the three β-sandwiches. Root mean square (rms) deviation of Cα positions of residues involved in the β-sandwiches is

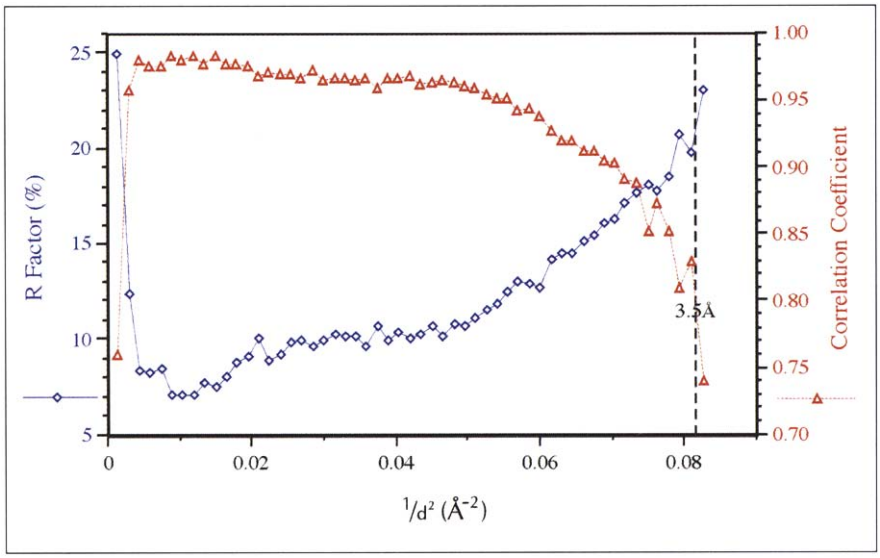

Fig. 2. A plot of R-factor (in blue), and correlation coefficient (in red) against $1/d^2$ (where d is the Bragg spacing) showing the agreement between the observed amplitudes and those produced by back-transforming the electron density from cycle 30 in the GAP real-space averaging (see text).

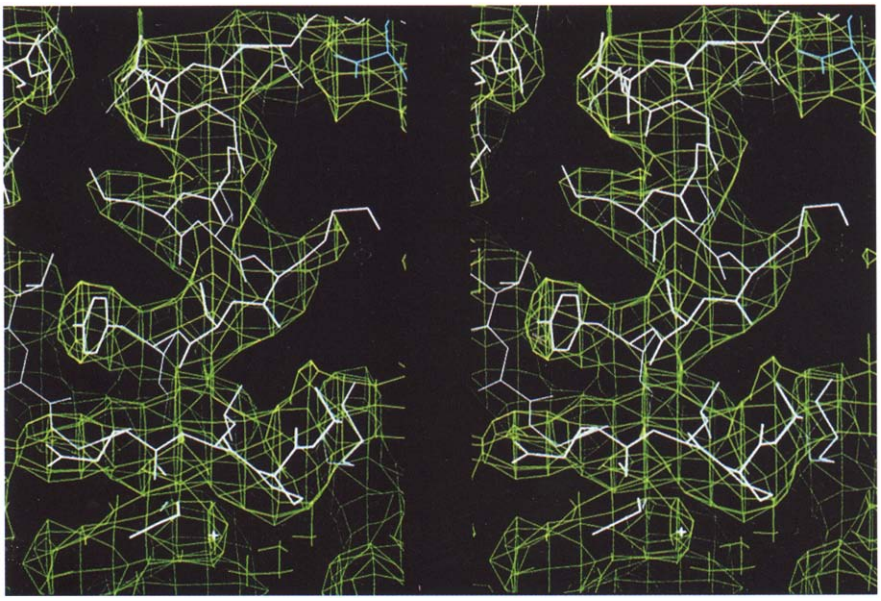

Fig. 3. A stereo view of a representative portion of the electron density map with amplitudes $2|F_{obs}| - |F_{av}|$ with phases from cycle 30 of GAP real-space averaging (as above) calculated at 3.5 Å resolution. The final model is shown in white.

Table 2. Stereochemistry, and residues included in final model of C-S8c1.

Refinement	
No. of independent reflections	79 016
No. of non-hydrogen atoms in refinement	5 197
Stereochemistry of model[a]	
RMS Δ bonds	0.012 Å
RMS Δ angles	2.0°
ΔB bonds	4.86 Å^2
ΔB angles	8.02 Å^2
Residues included in model	
VP1 (1–213)[b]	1–132, 157–211
VP2 (1–218)	1–218[c]
VP3 (1–220)[d]	1–220
VP4 (1–85)	15–39, 65–85

[a]RMSΔ bonds refers to the root mean square deviation from ideal covalent bond lengths. RMS Δ angles refers to the root mean square deviation from ideal covalent bond angles. RMS ΔB Bonds refers to the root mean square difference in isotropic B-value between covalently-bonded atoms. ΔB angles refers to the corresponding difference between covalently-bonded next nearest neighbours. [b]Numbering of residues is as for O_1BFS, therefore there are no residues 141–145. [c]There is no evidence for the position of the Glu6 side chain in VP2. It was therefore included as glycine in the final model. [d]Numbering relative to O_1BFS, there is therefore no residue 59 in this model.

0.3 Å, essentially the limit of accuracy of the data (Fig. 5). This is comparable with the rms deviation in Cα positions of the core residues seen in the comparison of poliovirus serotypes 1 and 3 [2]. Significant differences in Cα positions are observed only in the loops connecting the β-strands of these core regions and in the termini of the proteins (Fig. 5). The implications of these structural differences are discussed below.

The decreased order of the C-S8c1 crystals compared with those of O_1BFS (Fig. 5) may be related to the expansion of the cubic unit cell by 2.6 Å in C-S8c1. Crystal packing is mediated by a cluster of external residues of VP2 close to the crystallographic three-fold axes. In O_1BFS tight packing occurs with residues of VP2 stacking with equivalent residues in a neighbouring virion. In crystals of C-S8c1 substitutions of Pro→Gln at 195 and Val→Thr at 189 push the virions further apart. Hydrogen bonds are formed between the glutamine in one virus and the threonine in another such that the crystal lattice is held together, at each point of contact, by the six hydrogen bonds formed by these pairs around the three-fold axes.

Despite the decreased order of the C-S8c1 crystals we have been able to identify additional features in the electron density map which allow us to describe some regions of the capsid structure that were obscure in the O_1BFS analysis.

The three-fold annulus formed by amino-terminal residues of VP2

Capsid proteins VP2 and VP3 alternate around the icosahedral three-fold axes. Electron density (too diffuse to be unambiguously interpreted in O_1BFS) is seen around the icosahedral three-fold axes on the inside of the capsid, extending from residue 9 of VP2 (the last residue included in the O_1BFS model) to the three-fold axis and running back away from the three-fold axis over the internal surface of VP2 (Fig. 6a). A structure for these amino-terminal residues has not been previously described for any picornavirus. The model now includes all residues of VP2. The first six residues of VP2 run across the internal surface of the capsid towards the icosahedral three-fold axis before turning to follow an outward path (to a higher radius), parallel to and close to the three-fold axis, forming a tight core of three strands (Figs 6b and 6c). Residues 10–12 loop back towards the interior of the capsid placing residue 12 between residues 3 and 27 from the same copy of VP2. Residue Asp12 of VP2 (which is almost completely conserved amongst picornaviruses sequenced to date [22]) seems important in stabilizing the conformation of this loop, making hydrogen bonds

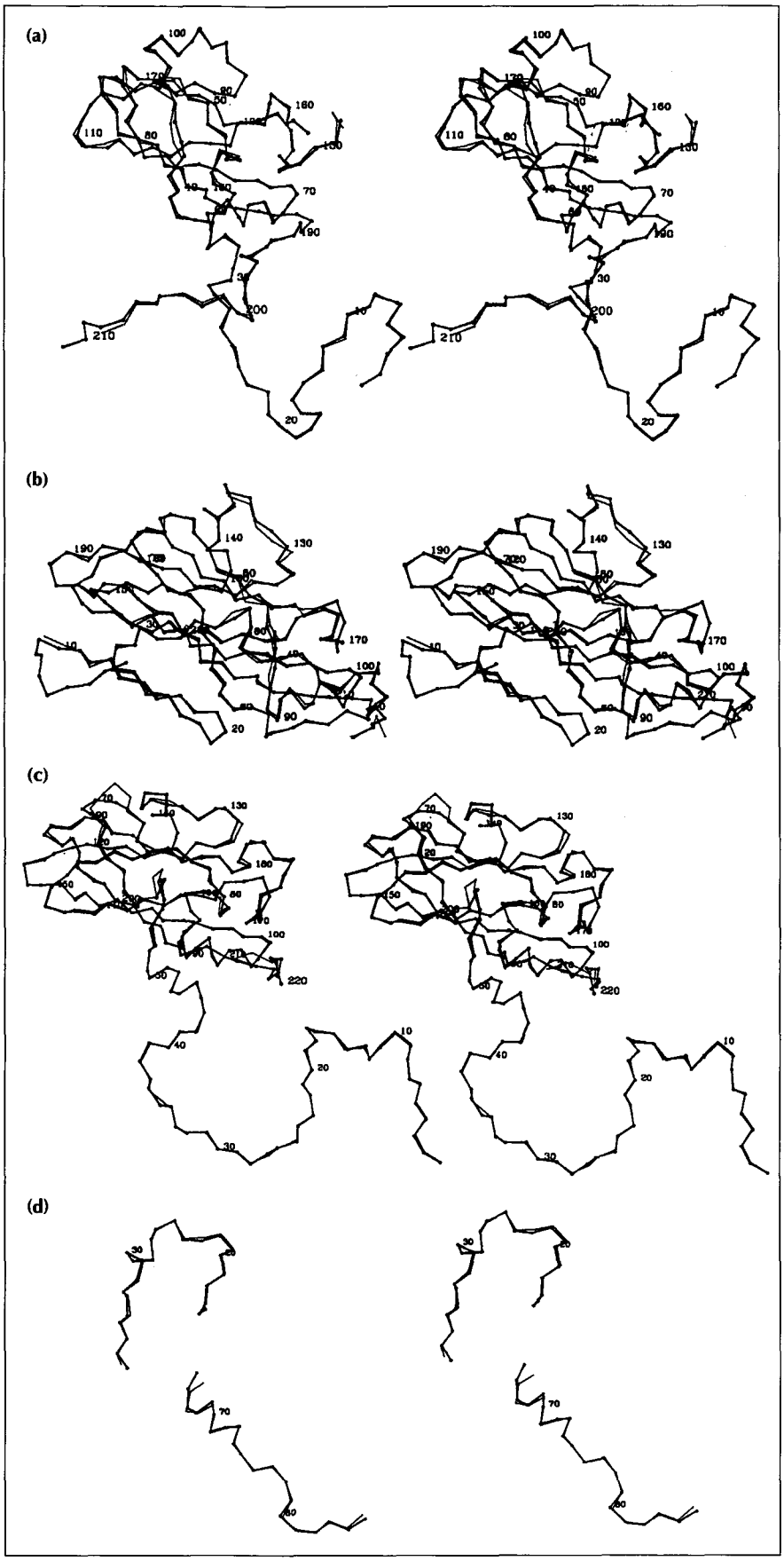

Fig. 4. Stereo views showing a superimposition of Cα traces of the individual capsid proteins of FMDVs C-S8cl (Cαs shown as black spheres linked by black bonds) and O_1BFS (thinner bonds) produced using MOPE (D Stuart, unpublished program). **(a)** VP1. **(b)** VP2. **(c)** VP3. and **(d)** VP4. Every tenth amino acid is labelled (residue labels are for O_1 numbering).

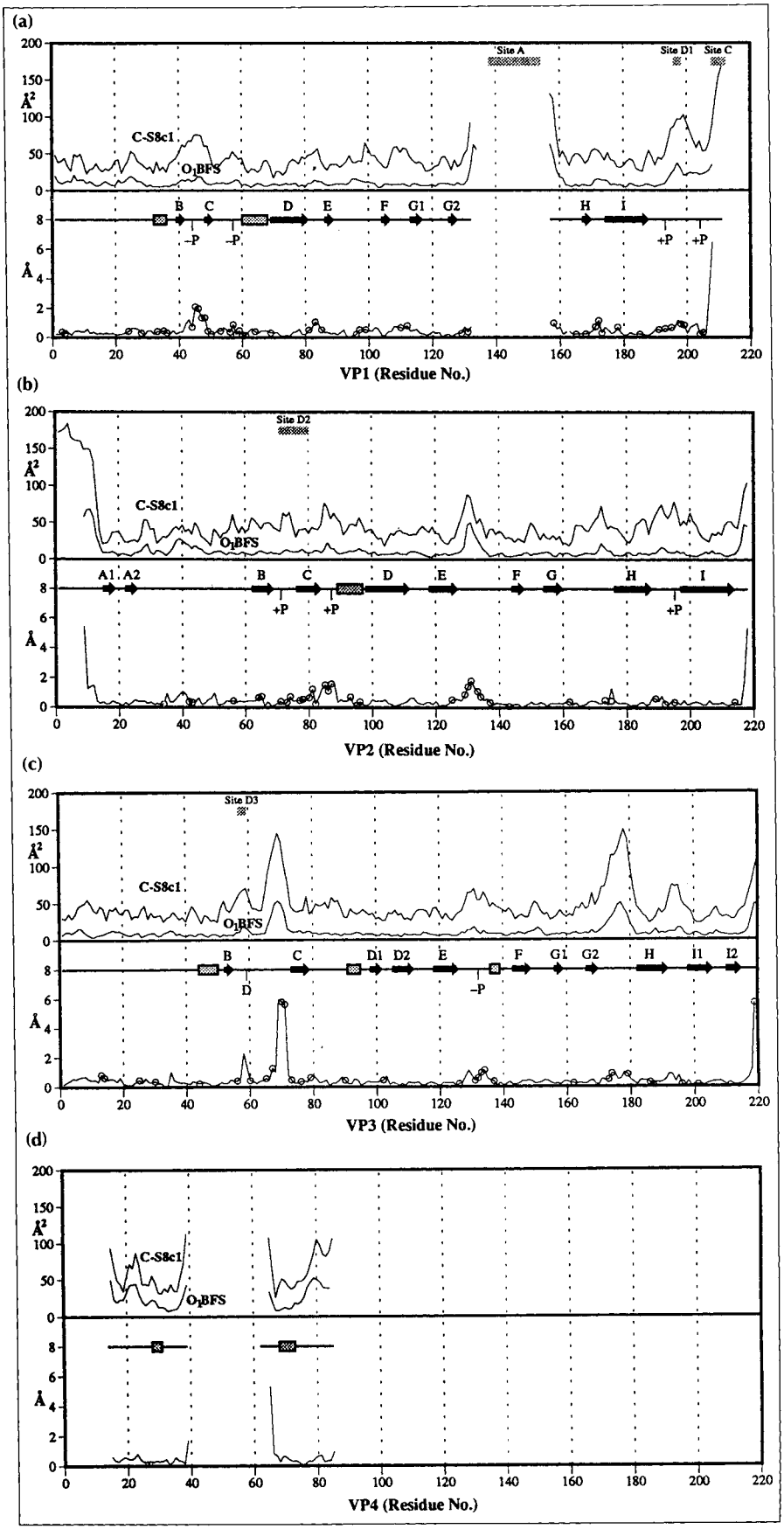

Fig. 5. Structural differences between C-S8c1 and O_1BFS. **(a)** VP1. **(b)** VP2. **(c)** VP3. **(d)** VP4. The upper part of each plot shows the main chain B-factors for C-S8c1 and O_1BFS. The lower plot shows root mean square deviations in Cα positions between C-S8c1 and O_1BFS for each capsid protein calculated using SHP (D Stuart, unpublished program). Positions of antigenic sites defined for C-S8c1 are shown as grey bars in the upper part of each plot, and sequence differences between the serotypes are shown as open circles in the lower part. Secondary structural elements (calculated using program DSSP [69]) are shown at the top of each lower plot, labelled according to the conventions defined in the text (β-sheets – black arrows, α-helices – grey boxes, +P – proline substitution, -P – proline deletion). The deletion at residue 59 of VP3 is marked D in (c).

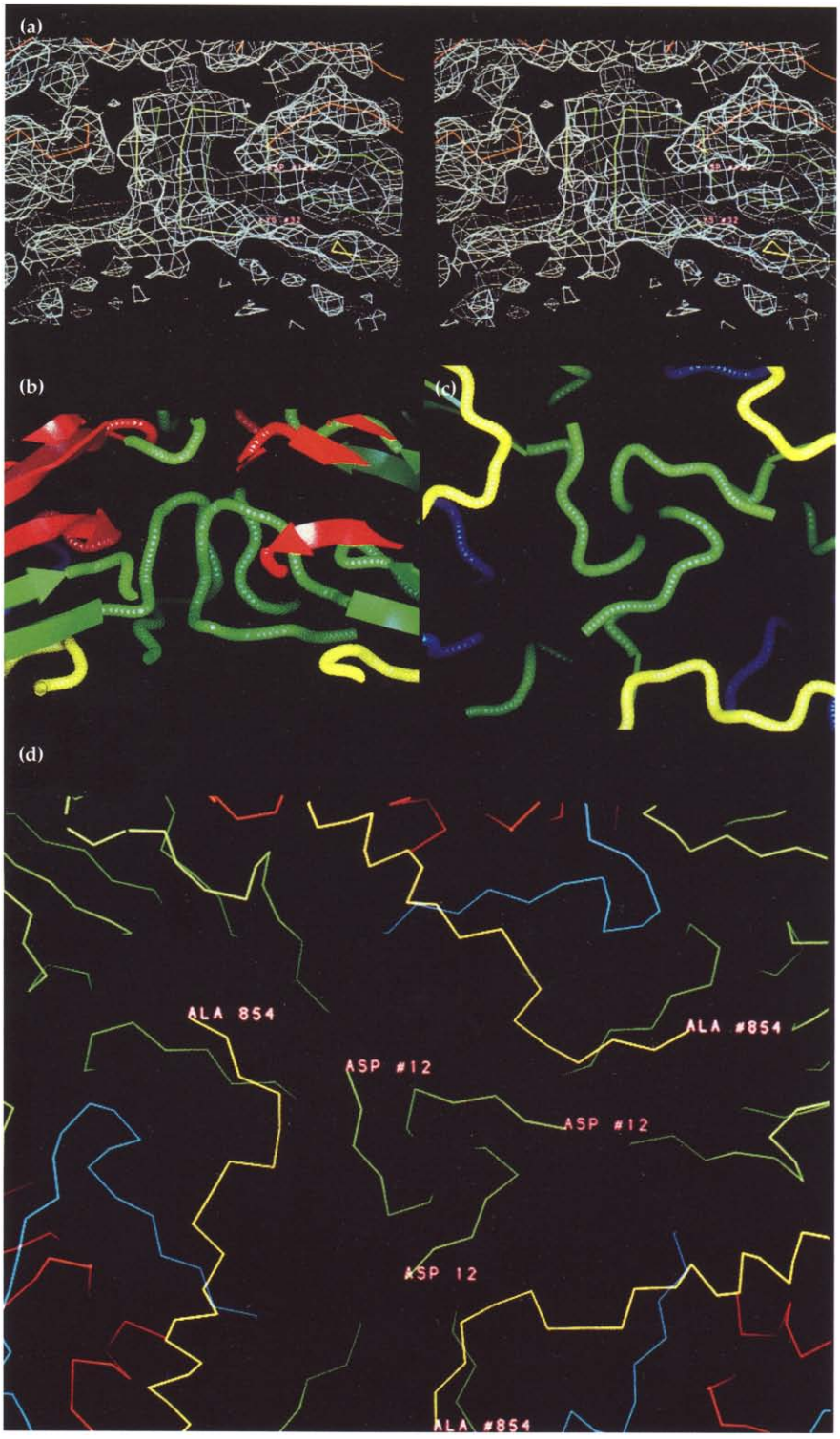

Fig. 6. Views of the internal structure of the virion at an icosahedral three-fold axis. **(a)** Stereo view of the electron density at the 3-fold axis. The view is similar to that shown diagrammatically in (b), and the protein chains are shown as Cα traces. **(b)** and **(c)** Cartoon representation of the capsid proteins around the three-fold axis of the virion. Two orthogonal views are shown ((b) perpendicular to the three-fold axis and (c) looking down the three-fold axis from the inside of the capsid). Proteins are coloured according to convention (VP1-blue; VP2-green; VP3-red; VP4-yellow). **(d)** A more distant view from the interior of the capsid looking down the three-fold axis (Cα trace of the capsid proteins coloured as above) with the symmetry related amino-terminal residues of VP2 and carboxyl-terminal residues of VP4 highlighted. The residues are numbered with the least significant digit denoting the polypeptide chain, thus 854 is residue 85 of VP4. Residues without a # in the residue number belong to a single biological protomer.

via side and main chain atoms to residues 12 and 3 of the same copy of VP2, as well as to residue 5 of a symmetry-related loop. This structure is stable in refinement, although the chemistry is less than ideal and B-factors for many atoms are still high ($\sim$150 Å^2). A map calculated with residues 1–12 of VP2 omitted from the phasing model confirmed the positioning of the main chain atoms, although due to the mobility of the protein in this region the density was somewhat diffuse, with little evidence for side-chain positions in the 'core' region close to the three-fold axis. Although the connectivity at residue Glu6 is not certain it agrees with that observed in mengovirus [23] and poliovirus [1]. We are therefore confident that the connectivity is correct, although the present model is not definitive. In the structure of C-S8c1, residues 1–4 of VP2 run towards

the three-fold axis, filling a shallow depression on the internal surface of the capsid and occupying a similar location to the amino-terminal extension of VP1 in poliovirus [1], resulting in a smooth internal surface.

Topologically similar (although more elaborate) β-annuli have previously been seen at the three-fold axes of RNA plant viruses [24,25]; these structures are however functionally different to the structure described here for FMDV as it is proposed that they play important roles in stabilizing the capsid (see below).

Extra density around the interior of the five-fold axis

Post-translational modification of proteins is often of great importance in determining correct localization, stability and functioning. Many viral proteins are found to be acylated with fatty acids and this is commonly important for localization on the plasma membrane of cells. Picornaviruses are not enclosed by a membrane but must still interact specifically with the cell membrane when entering the cell and during assembly of virus particles. Myristoylation of the amino terminus of VP4 (and its precursors) has been demonstrated in most picornavirus genera [26], the myristic acid (*n*-tetradecanoic acid) being covalently linked via an amide bond to the free α-amino group of the amino-terminal glycine of VP4.

The structure of this aliphatic moiety has been seen only in poliovirus to date [1,2,26]. The amino terminus of VP4 is located on the inside of the capsid close to the icosahedral five-fold axis and forms the innermost of three layers of protein which hold together the pentameric building block of the virus. The five myristate groups extend from the amino terminus of VP4, initially forming a tight cluster near the five-fold axis, then splaying apart and running to a higher radius, to enclose the twisted tube formed by the amino termini of VP3. Each myristate group interacts with several residues in VP3 and VP4. A hydrogen bond between Thr28 of VP4 and the myristate carbonyl (of a symmetry-related moiety) is observed. Moscufo and Chow [27] have demonstrated by site-directed mutagenesis the importance of the interaction of the myristate carbonyl with this residue in determining correct assembly of viable virions.

In FMDV C-S8c1, extra density (not accounted for by the model) is seen around the interior surface of the capsid close to the five-fold axes. Two views related by a 90° rotation are shown in Fig. 7. The five-fold environment of FMDV is somewhat different from that seen in poliovirus due to a canting of the VP1 β-barrel, the strands of the barrel being shifted approximately 3Å (outwards) compared with poliovirus [28]. Since the extra density observed (in the C-S8c1 map) is at the same radius as residue 1 of VP4 in the poliovirus model, there is more room to accommodate the hydrocarbon chains in FMDV. At present we cannot distinguish between two possible models which could both account for the extra density. In the first model the myristate group is assumed to occupy the depression on the inner capsid surface around the five-fold axis, as in poliovirus (the absence of density for this group being explained by the increased space available in FMDV). The myristate carbonyl may then be placed at a position equivalent to that seen in poliovirus, where it can hydrogen bond to the hydroxyl group of Asn23 of VP4 in an interaction analogous to the interaction with Thr28 of VP4 seen in the poliovirus model (Fig. 7a). The density observed would then be interpreted

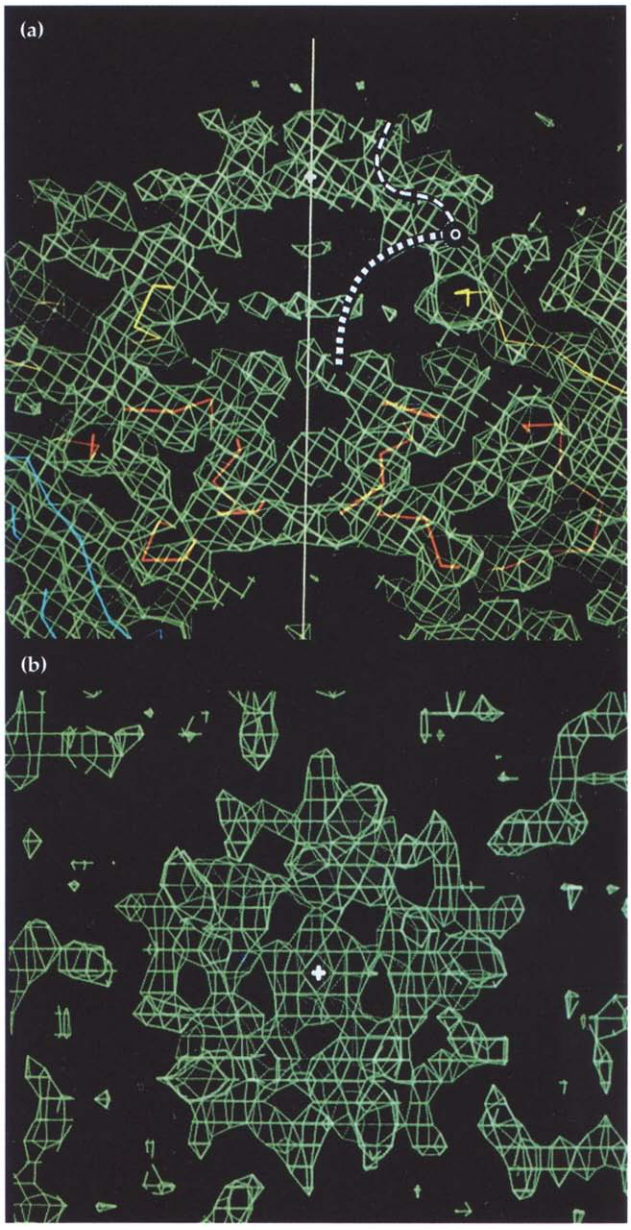

Fig. 7. The extra density seen around the interior of the icosahedral five-fold axes in the map calculated as described for Fig. 3. Two views related by 90° are shown. **(a)** View perpendicular to the five-fold axis (the five-fold axis is marked as a thin white line). The proposed location of the interaction between VP4 and the myristate carbonyl is indicated by the small white circle and the approximate path of a myristate chain in poliovirus (white dots), and possible route in FMDV (dashed white line) are indicated. **(b)** View looking down the five-fold axis from the interior of the virion (the five-fold axis is marked as a white cross).

as residues 6–1 of VP4 (with residue 6 the most internal). However, as no density can be seen for side-chains, we cannot unequivocally identify this feature as protein. Indeed the shape of the density favours the second model, in which the density corresponds to the myristate chains forming a twisted barrel with the five copies related by the icosahedral five-fold axis running inwards towards the virion centre, i.e. in the opposite direction to that observed in poliovirus (Fig. 7a). The myristate may then be stabilized by non-specific interactions with the RNA and the carbonyl oxygen can still hydrogen bond to residue 23 as described above. In both models the lack of continuous density for VP4 is explained by flexibility of the appropriate portion.

Our results therefore suggest that the fatty acid chains of the myristate moieties may be stabilized in FMDV by hydrogen bonds from a protein side-chain (Asn23 of VP4) to the myristate carbonyl in a broadly similar position to the interaction observed between the myristate moiety and Thr28 of VP4 in poliovirus.

The antigenicity of FMDV C-S8c1

The G–H loop and the carboxyl terminus of VP1 constitute independent antigenic sites that include continuous epitopes

Previous work has established that the antigenic site *A* within the VP1 G–H loop of FMDV C-S8c1 (VP1 residues 138–150; equivalent to positions 138–154 in type O) includes multiple, essentially continuous, overlapping epitopes [15,29,30]. The carboxyl terminus of VP1 (antigenic site *C*) is recognized by a weakly neutralizing MAb (7JA1). This reacts with VP1, with a synthetic peptide representing residues 192 to 209 (residues 196 to 213 in type O)[15] and with a recombinant fusion protein including amino acids 158 to 206 (162 to 210 in type O; A Rodriguez, *et al.*, unpublished data). We have confirmed the location of the continuous epitope recognized by MAb 7JA1 using antigen competition enzyme-linked immunosorbent assay (ELISA) with 15-mer synthetic peptides which span the sequence of VP1 of C-S8c1 from residue 41 to the carboxyl terminus (residues 1–40 are not solvent exposed). MAb 7JA1 recognized only the carboxy-terminal peptide (residues 195–209, equivalent to 199–213 in type O) (J Hernández, *et al.*, unpublished data). Thus, this epitope may span residues 195–206 of VP1 of C-S8c1. For FMDV of serotype O, it was shown that sites *A* and *C* are part of a single site which includes discontinuous epitopes [31,32], but no evidence of this has been seen for type C [15,29]. To further explore any possible connection between sites *A* and *C* in serotype C, antibody competition assays were carried out using a sandwich ELISA [33] to minimise virus distortion. No significant competition was observed between the MAbs directed to site *A* and the site *C* MAb 7JA1 (Fig. 8a, panels I to IV). Similar results were also obtained with a different type C FMDV, CGC-Ger/26 (Fig. 8a, panels V, VI), an early type C isolate which is genetically highly divergent from all other type C viruses [34]. Thus, antigenic sites *A* and *C* appear as topologically independent in serotype C. This is not inconsistent with the crystallographic observations, however the electron density is not sufficiently well defined to provide strong support (see below).

A major site, formed by discontinuous epitopes, involves parts of VP1, VP2 and VP3

Twelve of the 32 MAbs available, which neutralize FMDV C-S8c1, did not react with denatured capsid proteins or with peptides representing sites *A* or *C* [15] suggesting that they recognized discontinuous epitopes. We selected a representative sample of these MAbs (based on their different patterns of reactivity with field isolates [35]) to use in competition assays with MAbs directed to sites *A* and *C* (Fig. 8b). All of the MAbs which recognize discontinuous epitopes clustered in a single group (site *D*) distinct from those defined by MAbs of sites *A* or *C*. Partial competition was observed between most MAbs of sites *A* and *D*, suggesting spatial proximity of these two sites which leads to a degree of steric hindrance in binding antibody.

To locate the discontinuous epitopes on the viral capsid, 16 MAR mutants were selected from independent clones of FMDV C-S8c1 using six representative site *D* MAbs. The 16 site *D* MAR mutants (Table 3) and three previously described site *A* MAR mutants [29,30] were used in cross-neutralization assays with 10 of the 12 available MAbs against discontinuous epitopes of C-S8c1 [15] and with selected site *A* MAbs (Fig. 9). (The weak neutralizing activity of site *C* MAb 7JA1 precluded its use in these assays.) No substitution in MAR mutants of one of the sites (*A* or *D*) affected the reactivity of any MAb directed to the other site. This result was further confirmed in experiments using immunodot assays which showed that 10 MAR mutants with different substitutions in site *A* all reacted with site *D* MAbs (data not shown). Also, cleavage of the VP1 G–H loop affected many epitopes at site *A* but none of the site *D* epitopes (J Hernández, *et al.*, unpublished data). These findings suggest a functional independence of sites *A* and *D*.

Based on complete resistance to neutralization alone, the MAbs against discontinuous epitopes were divided into three groups (D_1, D_2, D_3, see Fig. 9). However, when one also considers partial resistance to neutralization, all discontinuous epitopes appear connected in a single site *D*, in agreement with the MAb-competition results. We have sequenced the entire capsid-coding region of six MAR mutants selected with five different site *D* MAbs which exhibited different patterns of neutralization. In addition, the relevant capsid segments were sequenced for the remaining 10 mutants (Table 3 and Fig. 9). Mutants selected with MAbs 1G5 or 2A12 (group D_1) repeatedly showed substitutions at residue 193 of VP1 (residue 197 in type O, Table 3 and Fig. 9) near the carboxyl terminus of VP1. Those selected with MAb 2A10 (group D_3) showed a substitution at residue 58 of VP3. Those selected with MAbs 2E5, 5H10 and

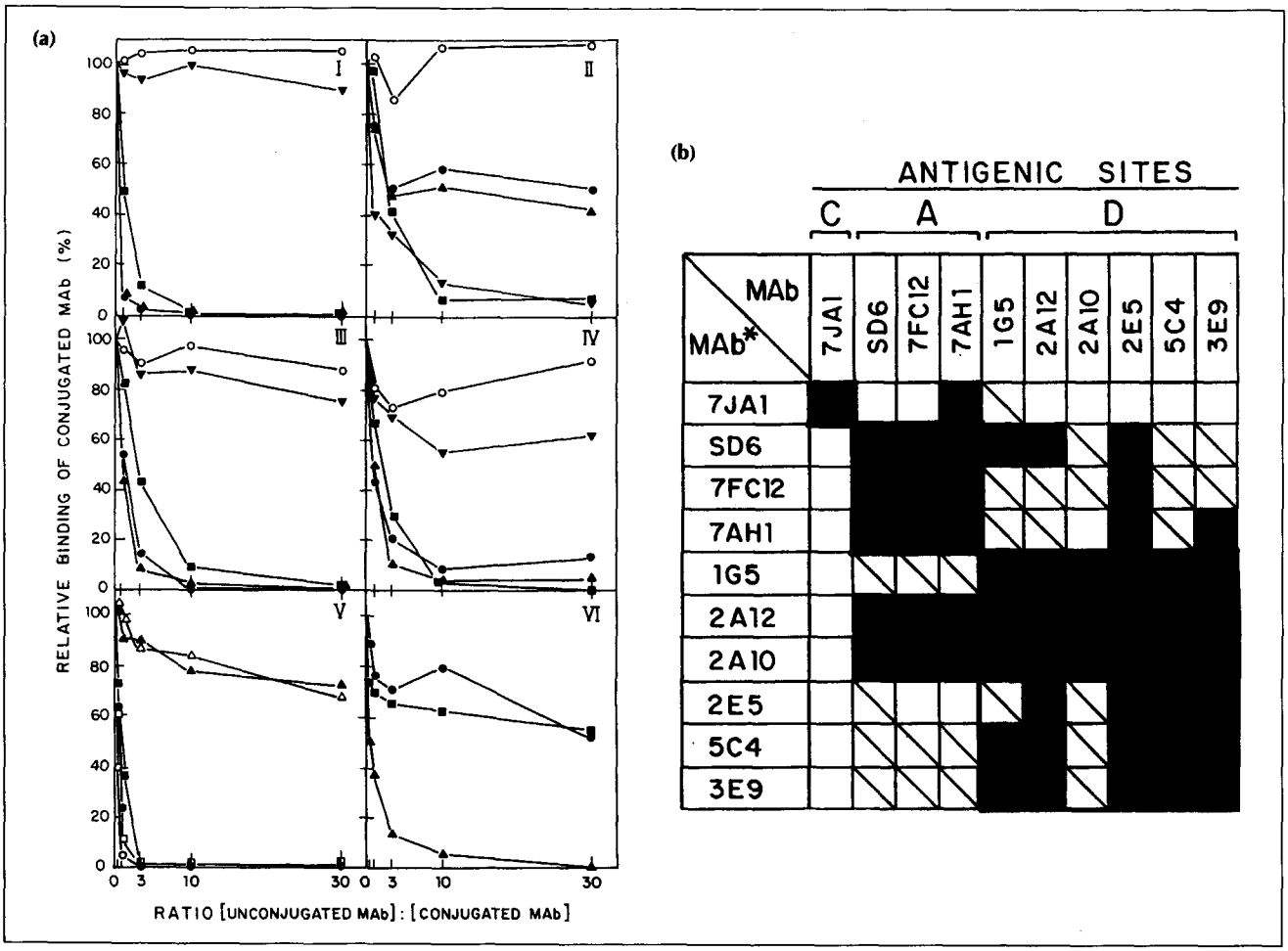

Fig. 8. (a). Competition of MAbs against sites *A* or C for the binding of FMDV of serotype C. Panels I-IV; C-S8cl was used as an antigen; peroxidase-conjugated MAbs SD6 (panel I), 7JA1 (II), 7FC12 (III), 7AH1 (IV), were competed by unconjugated SD6 (●), 7JA1 (▼), 7FC12 (▲), 7AH1 (■) or an unrelated MAb (Mab 28) elicited against respiratory syncytial virus (0). Panels V and VI, C GCGer/26 was used as antigen; peroxidase-conjugated MAbs 7AB5 (V, empty symbols), 7FC12 (V, filled symbols) or 7JA1 (VI) were competed by unconjugated 7AB5 (■ □), 7FC12 (● ○), or 7JA1 (▲ △). **(b)** nMAb competition for the binding to FMDV C-S8cl. Each conjugated MAb (MAb*) was competed by 1, 3, 10 and 30–fold its amount of each unconjugated MAb (MAb). The percent competition with a 30-fold excess of unconjugated MAb relative to the amount of active conjugated MAb is shown as a filled square for more than 90% competition, a hatched square for more than 60%, or as an empty square for less than 60%.

5C4 (group D_2) contained substitutions at residues 72 or 74 of VP2 within the BC loop or at residue 79 in the β-strand following this loop. One of the D_1 mutants (2A12-c3) had an additional mutation at the position (58 VP3) characteristic of site D_3. Because of this second replacement, mutant 2A12-c3 resembles the D_3 mutants (2A10-c1 and -c2) in its pattern of neutralization by MAbs against D_1 and D_3 (Table 3, Fig. 9).

Fig. 10 shows the location on the capsid structure of each antigenically relevant amino acid replacement in mutants selected with site *D* Mabs. The substitutions lie at highly exposed positions adjacent to each other and close to the three-fold axis of the virion within a single biological protomer (VP1 and VP2 from one icosahedral unit and VP3 from a neighbouring, symmetry related unit). The amino acids replaced cover an area slightly larger (30Å in diameter) than an antibody footprint. Site *D* lies close to the predominant location assigned to site *A* (Fig. 10), in agreement with the partial competition for binding observed between MAbs of site *A* and site *D*.

Some of the structural elements involved in site *D* are also antigenic in FMDV type A [36,37] and in other picornaviruses [38] such as poliovirus, rhinovirus, mengovirus and even a picorna-like plant virus [39]. The identification of another, complex antigenic site for FMDV type C involving all three solvent accessible capsid proteins connects functionally separated sites (sites 2 and 4) described in serotype O [40] and extends the surface that has been implicated in the antigenicity of FMDV. The smooth capsid of FMDV, with no canyons or pits separating antigenic protrusions, may render nearly the entire surface accessible to antibodies. Extension of the Mab mapping studies may therefore eventually blur the distinctions between the different sites and favour the view that the entire FMDV surface accessible to antibodies may prove antigenic [41]. This concept is supported by previous studies

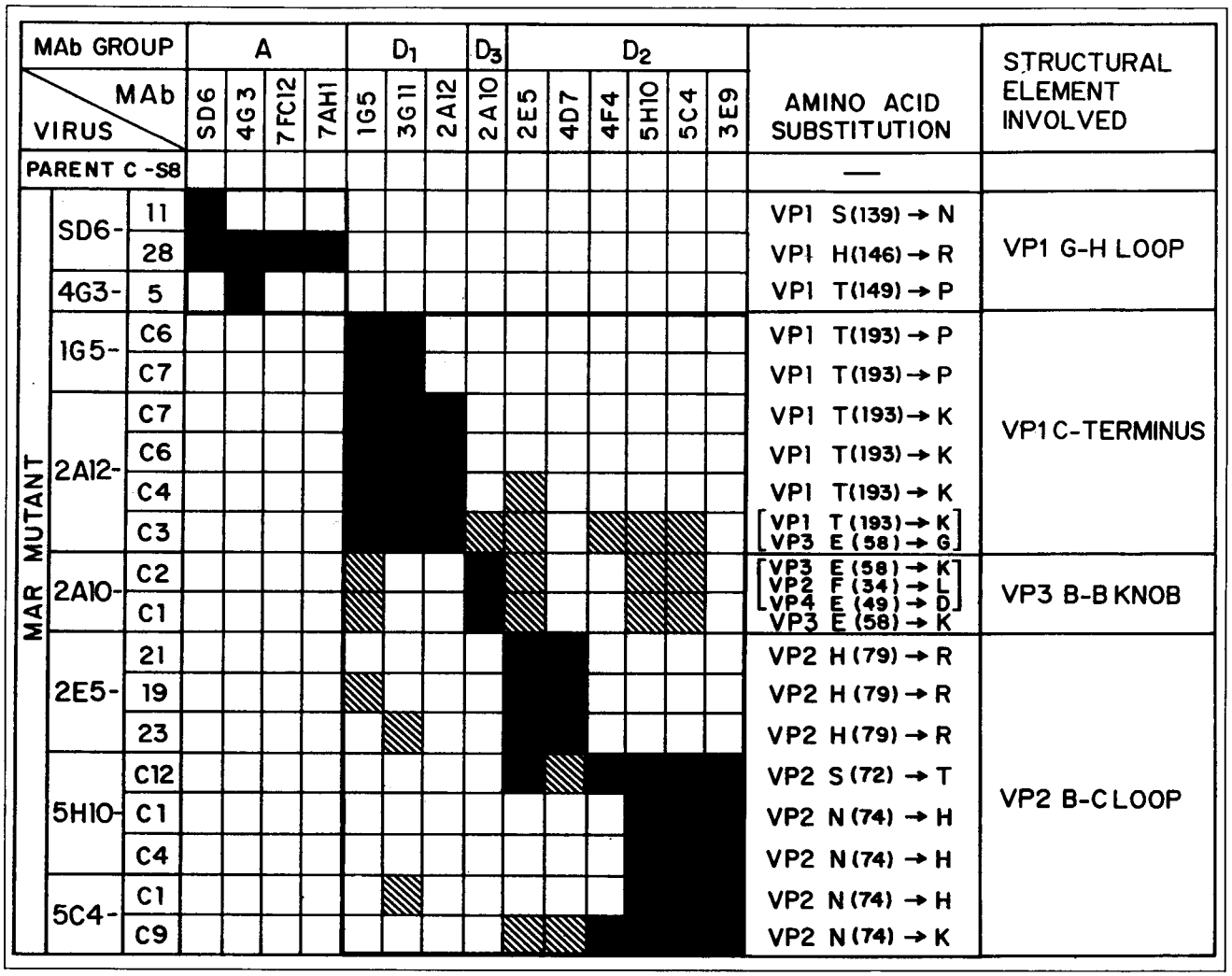

Fig. 9. Cross-neutralization patterns and amino acid substitutions of MAR mutants selected with MAbs directed to the epitopes in sites *A* and *D*. Sensitivity to neutralization was referred to that of the parent virus C-S8cl. For each MAb except 4G3 and 4F4, a concentration high enough to neutralize more than 90 % of the plaques of C-S8cl in an *in vitro* neutralization assay distinguished between sensitive mutants (empty square; > 70 % neutralization), partially resistant (shaded square; > 30 % neutralization) and resistant mutants (black square; < 30 % neutralization). For the weakly neutralizing MAbs 4G3 and 4F4 a concentration of MAb that neutralized more than 75 % of the plaques of C-S8cl distinguished between sensitive (empty square; > 50 % neutralization), partially resistant (shaded square; > 20 % neutralization), and resistant (black square; < 20 % neutralization). In most cases resistance (black square) indicated close to 0 % neutralization (under the conditions of the assay). The secondary structure elements where the substitutions were found are indicated.

with lysozyme [42] and the human growth hormone [43]. Although data from MAR mutants may suffer from limitations imposed by incompleteness, information on structural variability and solvent accessibility does not and can also be used to predict antigenic regions.

Conformational divergence, mobility, and the mechanism of antigenic change

For viruses like FMDV, against which the humoral response constitutes the main immune defence, it is important that areas of the capsid liable to attack by antibodies should be capable of antigenic change. In principle this can be achieved either by substitutions of antibody contact residues or by changes in protein conformation. Since such changes are usually associated with each other, we might expect antigenic sites to be correlated with regions of greatest conformational divergence between the two serotypes.

Fig. 5 confirms this expectation, in that all the sites identified in FMDV C-S8c1 (except site D_2) coincide with regions of greater than average rms deviation in Cα position, although in the case of site *A* (the G–H loop of VP1), the difference is not quantifiable since the loop is disordered in both viruses. In addition to these regions, the B–C loops of VP1 and VP3 and the E–F loop of VP2 exhibit very large conformational differences. Interestingly, antigenic residues have been identified in these loops either in type O [40] or A [36]. Thus, if all the available information on antigenic sites in FMDV is taken into account, variability in conformation of surface regions is seen to be an excellent predictor of potential antigenic change. Whether the

Table 3. Mutants of FMDV C-S8c1 selected with MAbs that recognize discontinuous epitopes.

MAb	Mutant frequency[a]	MAR mutant[b]	Mutation[c]	Substituted amino acid[d]
1G5	$\sim 10^{-4}$	1G5–c6	*A*(2143)→*C*	*VP1T*(193)→*P*
		1G5–c7	*A*(2143)→*C*	*VP1T*(193)→*P*
2A12	$< 10^{-6}$	2A12–c7	*C*(2144)→*A*	*VP1T*(193)→*K*
		2A12–c6	*C*(2144)→*A*	*VP1T*(193)→*K*
		2A12–c4	*C*(2144)→*A*	*VP1T*(193)→*K*
		2A12–c3	*C*(2144)→*A*	*VP1T*(193)→*K*
		"	*A*(1082)→*G*	*VP3E*(58)→*G*
2A10	$\sim 10^{-7}$	2A10–c2	*G*(1081)→*A*	*VP3E*(58)→*K*
		"	*A*(147)→*C*	*VP4E*(49)→*D*
		"	*T*(355)→*C*	*VP2F*(34)→*L*
		"	*A*(1341)→*G*	*SILENT*
		2A10–c1	*G*(1081)→*A*	*VP3E*(58)→*K*
2E5	$< 10^{-6}$	2E5–19	*A*(491)→*G*	*VP2H*(79)→*R*
		2E5–21	*A*(491)→*G*	*VP2H*(79)→*R*
		2E5–23	*A*(491)→*G*	*VP2H*(79)→*R*
5H10	$\sim 10^{-4}$	5H10–c12	*T*(469)→*A*	*VP2S*(72)→*T*
		5H10–c1	*A*(475)→*C*	*VP2N*(74)→*H*
		5H10–c4	*A*(475)→*C*	*VP2N*(74)→*H*
5C4	$\sim 10^{-4}$	5C4–c1	*A*(475)→*C*	*VP2N*(74)→*H*
		"	*C*(15)→*T*	*SILENT*
		"	*C*(673)→*T*	*SILENT*
		5C4–c9	*T*(477)→*G*	*VP2N*(74)→*K*

[a]Mutant frequency is given as the number of mutant plaques obtained divided by the total number of plaque forming units (pfu) plated in the presence of MAb. No mutant plaques were obtained with 2 × 10^6 total pfu and MAbs 2A12 or 2E5 in the assay. [b]All mutants were selected from independent plaque-purified clones of FMDV C-S8c1, except for 2A12-c7 and -c6 that were from a first clone and 2A12-c4 and -c3 derived from a second one. Mutant 2A10-c2 was isolated from uncloned C-S8c1. [c]Numbering is from the first nucleotide of P1 of C-S8c1 corresponding to the beginning of the gene VP4 to the last (2193) nucleotide corresponding to the end of the gene VP1. [d]C-S8c1 numbering. Residue 193 of VP1 equivalent to 197 in O_1BFS. The entire capsid region (nucleotides 1 to 2193) of mutants 1G5-c6, 2A12-c3 and -c7, 2A10-c2, 2E5-21 and 5C4-c1 was sequenced. For other mutants the relevant segments were sequenced: 1G5-c7, 2A12-c4 and c-6: nucleotides 1891–2193; 2A10-c1: nucleotides 202–449 and 930–1170; 2E5-19 and 23, 5H10-c1, -c4 and -c12 and 5C4-c9: nucleotides 363–670. The entire capsid of mutant SD6-28 (Fig. 9) was also sequenced. Sequence ambiguities were found only in nucleotides 1183 (any virus), 928 and 1247 (SD6-28) corresponding to amino acid positions 92, 7 and 113 of VP3 respectively (C-S8c1 numbering).

serotypic differences in antigenicity reflect actual immunological preferences, or simply incompleteness of the panels of MAbs and MAR mutants used is presently unclear.

Fig. 5 shows that there is a marked correlation between residue mobility (as judged from crystallographic B-factors) and conformational differences between O_1BFS and C-S8c1. A correlation coefficient, C_{BD}, has been calculated to investigate the link between mobility and positional differences between two proteins (Materials and methods) [44]. Acharya *et al.* [44] have compared the structures of two species of α-lactalbumin using this measurement. These proteins share 92% sequence identity and both structures are refined against high resolution data (both at 1.7 Å) — the atomic B-factors and positions are therefore well defined. C_{BD} is 0.82 for the α-lactalbumins. For O_1BFS *versus* C-S8c1, C_{BD} is 0.73. This emphasizes the linkage between residue mobility and conformational change (given the lower degree of sequence identity between the viruses).

Similarly a correlation C_{BB} between atomic B-factors for equivalent atoms in the two structures may be calculated (Materials and methods). The value of C_{BB} for O_1BFS and C-S8c1 is 0.79 (this result is independent of the starting B-factors for the C-S8c1 refinement), compared to 0.84 for the α-lactalbumins [44]. This strong correlation between the B-factors for the O_1BFS and C-S8c1 structures indicates that even with X-ray data of limited resolution we may interpret B-factors with confidence. Links between protein mobility (as measured by crystallographic B-factors) and antigenicity have previously been made [45–47]. These are complicated by the fact that antigenic residues will be surface oriented and will therefore be more mobile than the core protein regions. As quantified in the correlation coefficient, we see that mobility and conformational change are strongly linked by the fact that these will be characteristic of less conformationally constrained regions of the protein. This lack of constraint gives greater tolerance to different amino acid substitutions, facilitating antibody escape.

In contrast to all other antigenic sites, site D_2, located in the B–C loop of VP2, is antigenic in both type C and type O but does not exhibit an rms deviation in Cα positions significantly above the level of experimental accuracy of the coordinates. Although the main chain protein conformation in this region is conserved between the two viruses, the sequences are very different and the site will therefore appear different (in terms of surface shape and chemical nature) to an antibody attempting to recognize this region. A careful analysis of the hydrogen-bonding pattern in this site demonstrates that antigenic change is accomplished by mutations occurring at positions with surface oriented side-chains (Table 4) not involved in interactions with the surrounding protein (Fig. 11). In this site there is only one position where the side-chain forms a hydrogen bond (His79) at which a substitution is seen. The only replacement seen at this position is His→Arg and modelling of this change suggests the hydrogen bond can be conserved. Likewise, residue 193 of VP1 (residue 197 O_1BFS numbering) within site D_1 is the most exposed amino acid in this part of the carboxyl terminus, and is also the only one of the exposed residues in this segment not involved in interactions with the surrounding protein. Thus, it appears that structural constraints limit those substitutions allowed in response to immunological pressure.

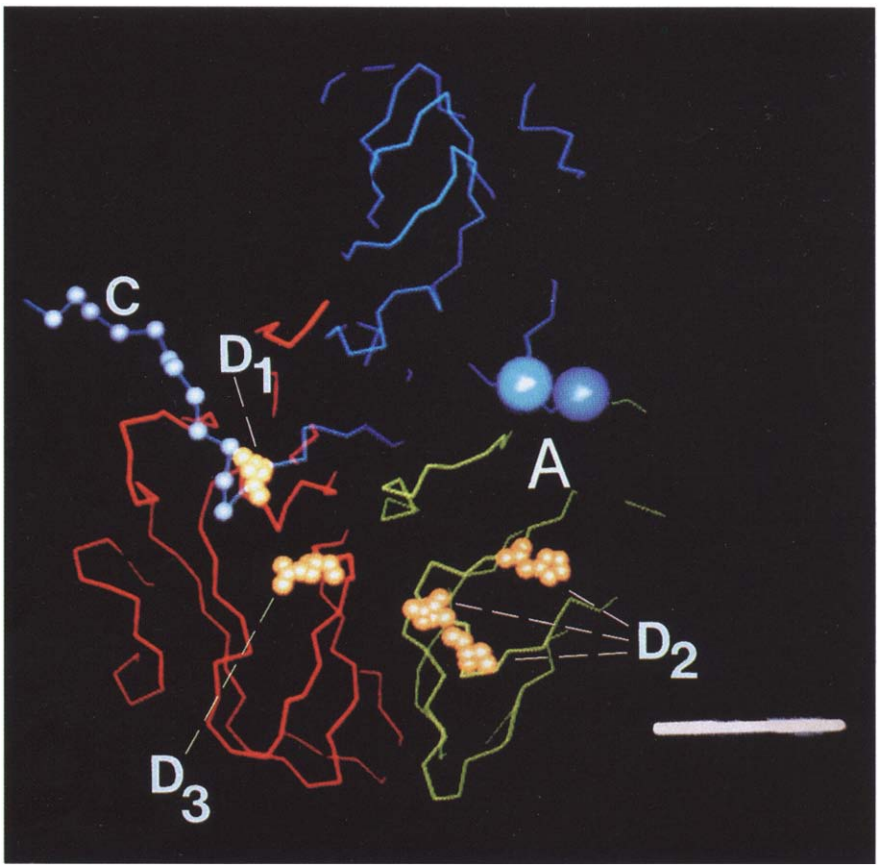

Fig. 10. Location of Sites *A*, *C*, and *D*, on the capsid. For simplicity a single biological protomeric unit is shown using standard colouring (VP1 - blue; VP2 - green; VP3 - red). A 20 Å white bar is shown (bottom right) to give the scale. Site *D* is indicated in yellow by all atom, space filling representations of the residues altered in MAR mutant viruses defining this site. Sites D_1, D_2 and D_3 which make up this site are indicated in white. Site *C* has been identified by peptide mapping and is indicated by cyan spheres at the Cα positions of the sequence (195–206, C-S8cl numbering) corresponding to a reactive peptide. Site *A* is less well ordered, and no detailed model has been constructed for this loop. The ordered termini of this loop are shown as large blue spheres, and the region likely to accommodate the loop indicated by 'A'. It must be remembered that in the entire virion a symmetry related copy of site *C* will lie close to these termini (but somewhat above, as shown in this view).

Table 4. H_2O Accessibilities of residues in B–C loop of VP2 (site D_2)

Residue number (VP2)[a]	Residue type	H_2O accessibility[b]
70	Val	39.0
71	Pro	33.6
72	Ser	92.8
73	Gln	25.5
74	Asn	89.3
75	Phe	31.3
76	Gly	5.8
77	His	79.0
78	Met	35.2
79	His	52.0
80	Lys	76.1[c]

[a]Residues 72, 74 and 79 or residues 70, 74, 77 and 79 were found repeatedly substituted in MAR mutants of C-S8c1 or in field antigenic variants of serotype C [35], respectively. [b]Accessibilities calculated by the method of Lee and Richards [68]. A probe of radius 1.4 Å is rolled over the surface of the protein, the accessible area being defined as the continuous path of the centre of this probe. [c]Although the accessible area for this residue is large the residue is not surface directed; it lies across the capsid surface (a fully exposed lysine would have an H_2O accessible area of 218.5 Å^2). Access to this residue by a large molecule such as an antibody may also be restricted by residue 131 (VP2) from a neighbouring loop, although this residue does not lie sufficiently close to restrict access of the H_2O probe.

Flexibility of the VP1 G–H loop

Unexpectedly the VP1 G–H loop in C-S8c1 is again found to be significantly less well ordered than other surface exposed loops, despite lacking the disulphide bond known to destabilize this structure in O_1BFS [14] and despite being four residues shorter in CS8-c1 than in O_1BFS (there is a deletion after residue 140 of VP1). No detailed model has been constructed for residues 133 to 156 (equivalent to 133–152 using a C-S8c1 numbering scheme). The missing region corresponds closely to the disordered portion in O_1BFS and to the residues involved in antigenic site *A* of C-S8c1 (residues 138–154, equivalent to 138–150 using a C-S8c1 numbering scheme [15]). Analysis of redissolved crystals confirms that there has been no proteolysis of VP1 (data not shown).

Although the loop appears relatively disordered, low level density for some of the main chain atoms can be seen. The electron density is discontinuous in this region. However, a crude model based on the reduced O_1BFS [14] structure has been constructed and explains most of the observed electron density. The approximate position of the loop, based on these observations is shown in Fig. 10. The loop conformation adopted in C-S8c1 appears somewhat different to that seen in the reduced O_1BFS structure (not unexpectedly, since within the loop 50 % of the amino acids are different and there is a four residue deletion) but the chain occupies a similar region of the capsid surface, lying predominantly over VP2 in both cases. This in-

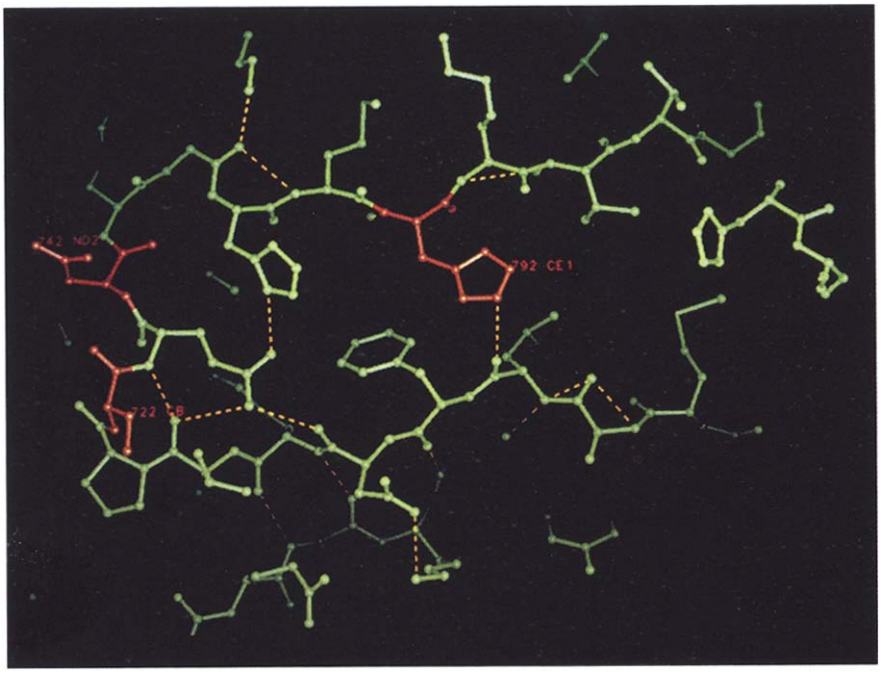

Fig. 11. Close up of a specific site, D_2, showing the hydrogen-bonding pattern. All non-hydrogen atoms are shown in a ball and stick representation. The three amino acids at which substitutions occur in MAR mutants are highlighted in red (and labelled with the residue number the least significant digit of which refers to the protein identity).

dicates that the loop residues spend at least part of the time near the viral two-fold axis and away from the carboxyl terminus of VP1 (site *C*). This appears to differ from the native type O_1 structure where indirect evidence suggests that the loop residues are mainly located over VP1, near the viral five-fold axis, close to the carboxyl terminus of VP1 [13]. A different location of antigenic site *A* in FMDVs of serotypes O and C provides a rational explanation for the finding of a single discontinuous site in type O (involving both the VP1 G–H loop and the VP1 carboxyl terminus) [31,32,40], and of two independent, continuous antigenic sites in type C as evidenced by MAb binding and competition experiments. We cannot rule out the possibility that other antibodies could recognize discontinuous epitopes of type C involving both the G–H loop and the carboxyl terminus of VP1. However, this may be an infrequent case, as none of the 31 MAbs tested for C-S8c1 appears to recognize such an epitope.

Conservation of disorder between FMDVs of type O and C suggests flexibility of this region is advantageous to the virus. The importance of the VP1 G–H loop in FMDV is well established. Numerous studies suggest it is perhaps the most important antigenic feature on the virion surface ([48–50], reviewed in [51]). Sequence analyses show that the G–H loop is one of the most variable segments of the virus capsid (reviewed in [22,51]). Clearly a very flexible loop places fewer structural constraints on the types of amino acid found within it. Preservation of the flexibility of the VP1 G–H loop of FMDV allows considerable sequence, and thus antigenic, diversity [15,52,53].

Biological implications

Foot-and-mouth disease virus (FMDV) causes an economically important disease of livestock. It is highly varied antigenically, complicating the task of controlling the disease by vaccination. Our structure, which represents a second serotype of FMDV, provides insights into the mechanism of viral maturation, and the mechanism of antigenic change.

The structure of type C FMDV reveals the complete amino terminus of VP2. The cleavage of VP4 from VP2 during the final stage of picornavirus assembly is essential for capsid function. Here we show that, after cleavage, a conformational change separates the cleaved ends by approximately 31Å. The coiled structure of the VP2 amino terminal regions and the lack of stabilizing interactions between them and the interior of the virion suggests that these are the residues that rearrange after cleavage. We speculate that this structure for the amino terminal residues of VP2 may not form unless RNA has been assembled into the virion, forcing these residues into the depression around the three-fold axis.

We also show here that data on the structural variability and solvent accessibility of regions of the virus can be used to predict their antigenicity.

Analysis of mutations in these regions that confer resistance to neutralization by monoclonal antibodies indicates that substitutions are generally restricted to residues with exposed side-chains not involved in interactions with surrounding protein; thus, structural constraints appear to 'filter' the substitutions allowed in response to selective pressure. This may explain the common observation that the same amino acid substitution is repeatedly found in independently derived antibody resistant mutants of viruses [29].

The RGD tripeptide, which is critical for receptor binding and is highly conserved, is located within a hypervariable, highly antigenic surface loop. The FMDV receptor is unknown, but several lines of evidence indicate that it may be an integrin [9, 12, 54, 55]. In all known structures of RGD-containing integrin-binding proteins [56–60] the RGD is found at the tip of a flexible, highly exposed loop. The similarity with the VP1 G–H loop is striking, reinforcing the expectation that the cellular receptor(s) for FMDVs will belong to the integrin family. Since it is essential for the virus to allow sequence variability around the RGD, and since surface mutations are restricted, the observed flexibility in this loop may be important both for receptor recognition and for antigenic variation.

Materials and methods

Virus growth, purification and crystallization

Growth and purification of virus for crystallization followed standard procedures as described [16]. Crystals of FMDVs C-S8c1 and SD6-6 grew by vapour diffusion from 9.5–11.5% saturated $(NH_4)_2SO_4$ in the presence of 10 mM dithiothreitol [16].

FMDV C-S8c1 data collection

Crystals were mounted at Pirbright in quartz capillary tubes and data were collected at the SERC Synchrotron Radiation Source, Daresbury, following agreed disease security protocols. All data were collected on station 9.6 using radiation of wavelength 0.89 Å. The temperature at the crystal was approximately 17°C and data were recorded on photographic film (CEA Reflex 25) using the oscillation method. A crystal to film distance of 185.6 cm enabled data to be collected to a resolution slightly exceeding 3.5 Å. An oscillation range of 0.5° per exposure was used. Exposure times were between 12.5 and 15 min (with the machine operating at 2GeV, current between 206 and 150 mA). The photographic images were digitized on a 50 × 50 μm raster using an Optronics P-1000 microdensitometer (0–2 OD) and processed on a VAX computer as described [20].

FMDV SD6-6 data collection

Data were collected on station 9.6 of the SRS Daresbury using the Rigaku RAXIS II image plate. Of five crystals available for analysis only four diffracted. However, 24 images were collected (a maximum of eight images from one crystal) with an exposure time of only 1 min (due to the increased sensitivity of the image plate compared with film and the increased flux of the station after installation of a new mirror). SD6-6 crystallized isomorphously with C-S8c1. Data were processed using the MOSFLM program package (A Leslie unpublished program). Processing statistics are shown in Table 1. This SD6-6 data scaled to the C-S8c1 data with $R_C = 17.8\%$ and C = 0.89, however there was relatively little overlap between the data collected in the two data sets and these statistics were for only 39 995 common reflections.

Phase determination and model building

The procedures used for phase determination followed those described [20]. Model building was performed using the program FRODO [61] on an Evans and Sutherland ESV-10 graphics workstation.

Model refinement and analysis

All refinement was performed using the X-PLOR program [18], versions 2.2, 3.0 and 3.1, using only positional and B-factor refinement. Throughout the refinement strict five-fold non-crystallographic constraints were enforced, both on the positions of atoms and on the individual isotropic temperature factors to ensure a satisfactory ratio of observations to parameters. Both averaged and unaveraged $|F_{obs}| - |F_{calc}|$ and $2|F_{obs}| - |F_{calc}|$ maps were calculated. A simple bulk solvent correction was applied (as implemented in X-PLOR), with the solvent density set to $0.32e^-$ and a B-factor of 110 Å^2 to smooth the edges of the mask. All measured data were included throughout the refinement process, no matter how weak (negative intensities were treated with the program TRUNCATE [62]).

A correlation coefficient may be calculated to link residue mobility (as judged by crystallographic B-factors) and conformational differences between O_1BFS and C-S8c1 [44]. This takes the form:

$$C_{BD} = \frac{\sum_j((B_{j,1} - \langle B_1 \rangle) + (B_{j,2} - \langle B_2 \rangle)) \cdot (D_j - \langle D \rangle)}{\left[\sum_j((B_{j,1} - \langle B_1 \rangle) + (B_{j,2} - \langle B_2 \rangle))^2 \cdot \sum_j (D_j - \langle D \rangle)^2\right]^{1/2}}$$

where $D_j = X_{1,j} - X_{2,j}$, and X_j is the position of atom j (after superimposition of structures 1 and 2); B values are isotropic temperature factors and the sum Σ_j represents the sum over atoms C, O, N, Cα and Cβ. Similarly the B-factors for the two viruses may be correlated:

$$C_{BB} = \frac{\sum_j (B_{j,1} - \langle B_1 \rangle)(B_{j,2} - \langle B_2 \rangle)}{\left[\sum_j (B_{j,1} - \langle B_1 \rangle)^2 \cdot \sum_j (B_{j,2} - \langle B_2 \rangle)^2\right]^{1/2}}$$

Colour plates were produced using either FRODO [61] or O [63].

Monoclonal antibodies

The neutralizing MAbs used were elicited against FMDV serotype C. They have been described [15,30,52,64]. For competition assays, MAbs were purified by protein A-sepharose chromatography and/or ammonium sulphate precipitation (45% saturation). They were labelled with peroxidase by the periodate method [65]. Both unlabelled and labelled purified MAbs were tested in a sandwich ELISA to estimate their reactivity with FMDV.

Antibody competition assays

A sandwich ELISA [33] was used. Purified IgG from a pig immunized with FMDV C-S8c1 was adsorbed overnight at 4°C to ELISA plates. After washing of the wells with phosphate-buffered saline

(PBS), 3% bovine serum albumin in PBS was added and incubation continued for 2 h at room temperature. Then a five-fold dilution of supernatant from cell cultures infected with FMDV C-S8c1 was added. After 2 h at room temperature the wells were washed twice with PBS and mixtures containing a fixed, non-saturating amount of labelled MAb and different amounts of unlabelled MAb were added. For each labelled MAb, the amount of the same unlabelled MAb required for 50% competition was previously estimated, and this amount, or three-fold, ten-fold or thirty-fold this amount of each unlabelled MAb was used in the competition experiment. Controls without unlabelled antibody were also done. Incubation was for 90 min at room temperature. After 12 washes with 0.1% Tween-20 in PBS, the enzymatic reaction was carried out using o-phenylenediamine as a substrate. Absorbance was read at 492 nm. Backgrounds without virus ($A_{492} < 0.1$) were subtracted. An alternative method involved a first incubation with unlabelled MAb and a second one with labelled MAb. This was tested with MAb SD6, and provided the same results as the standard protocol.

MAb resistant mutants

They were isolated essentially as described [29]. Independent plaque-purified clones derived from C-S8c1 [10^5 to 10^7 plaque forming units (pfu)] were incubated with MAb and plated in the presence of the same MAb. A single plaque of virus was picked, incubated again with MAb, plaque-purified twice and finally amplified to about 10^{10} pfu. For mutants selected with MAbs 2E5 and 2A12 the whole progeny obtained in the first selection were used in the subsequent steps.

Neutralization assays

A plaque-reduction assay as described in [30] was carried out using two serial 10-fold dilutions of supernatant of hybridoma culture or ascitic fluid (depending on the MAb) in duplicate.

Nucleotide sequencing of viral RNA

Virions were purified through a sucrose cushion followed by centrifugation in a sucrose gradient. The RNA was extracted as previously described [66] and sequenced by primer extension and dideoxy chain termination as in [67] with minor modifications. The sequences of the primer oligonucleotides used were complementary to nucleotides 186–203, 309–325, 481–499, 685–704, 943–961, 1189–1209, 1417–1436, 1677–1692, 1830–1847, 2037–2056 of the capsid region (P1, 2193 nucleotides) and 35–54 of region P2 of FMDV C-S8c1 RNA.

Atomic coordinates have been deposited with the Brookhaven Protein Data Bank.

Acknowledgements: We thank D Goodrich for his time on data collection trips as disease security officer; the staff of the Synchrotron Radiation Source, SERC Daresbury Laboratory for practical assistance; R Bryan, R Esnouf and others from the LMB and IAH for their support; H Barahona (CPFA) and C Palomo (CNMVIS) for providing some MAbs. Work at CBM was supported by CICYT (PB91-0051-C02-01) and Fundacion Ramon Areces; JH is a predoctoral fellow from Comunidad Autonoma de Madrid; EF was supported by the MRC; SL, RA, WB and SC were supported by the AFRC.

References

1. Hogle, J.M., Chow, M. & Filman, D.J. (1985). Three-dimensional structure of poliovirus at 2.9 Å resolution. *Science* **229**, 1358–1365.
2. Filman, D.J., Syed, R., Chow, M., Macadam, A.J., Minor, P.D. & Hogle, J.M. (1989). Structural factors that control conformational transitions and serotype specificity in type 3 poliovirus. *EMBO J.* **8**, 1567–1579.
3. Rossmann, M.G., *et al.*, & Vriend, G. (1985). Structure of a human common cold virus and functional relationship to other picornaviruses. *Nature* **317**, 145–153.
4. Kim, S., *et al.*, & McKinlay, M.A. (1989). Crystal structure of human rhinovirus sterotype 1A (HRV1A). *J. Mol. Biol.* **210**, 91–111.
5. Oliveria, M.A., *et al.*, & Rossmann, M.G. (1993). The structure of human rhinovirus 16. *Structure* 1, 51–68.
6. Luo, M., *et al.*, & Palmenberg, A.C. (1987). The atomic structure of mengo virus at 3.0 Å resolution. *Science* **235**, 182–191.
7. Grant, R.A., Filman, D.J., Fujinami, R.S., Icenogle, J.P. & Hogle, J.M. (1992). Three-dimensional structure of Theiler's virus. *Proc. Natl. Acad. Sci. USA* **89**, 2061–2065.
8. Luo, M., He, C., Toth, K.S., Zhang, C.X. & Lipton, H. (1992). Three-dimensional structure of theiler murine encephalomyelitis virus (BeAn strain). *Proc. Natl. Acad. Sci. USA* **89**, 2409–2413.
9. Acharya, R., Fry, E., Stuart, D., Fox, G., Rowlands, D. & Brown, F. (1989). The three-dimensional structure of foot-and-mouth disease virus at 2.9 Å resolution. *Nature* **337**, 709–716.
10. Colonno, R.J., Candra, J.H., Mizutani, S., Callahan, P.L., Davies, M. & Murko, M.A. (1988). Evidence for the direct involvement of the rhinovirus canyon in receptor binding. *Proc. Natl. Acad. Sci. USA* **85**, 5449–5453.
11. Olson, N.H., *et al.*, & Rossmann, M.G. (1993). Structure of a human rhinovirus complexed with its receptor molecule. *Proc. Natl. Acad. Sci. USA* **90**, 507–511.
12. Fox, G., Parry, N.R., Barnett, P.V., McGinn, B., Rowlands, D.J. & Brown, F. (1989). Cell attachment site on foot-and-mouth disease virus includes the amino acid sequence RGD (arginine-glycine-aspartic acid). *J. Gen. Virol.* **70**, 625–637.
13. Parry, N., *et al.*, & Stuart, D. (1990). Structural and serological evidence for a novel mechanism of immune evasion in foot-and mouth disease virus. *Nature* **347**, 569–572.
14. Logan, D., *et al.*, & Fry, E. (1993). Structure of a major immunogenic site on foot-and-mouth disease virus. *Nature* **362**, 566–568.
15. Mateu, M.G., *et al.*, & Domingo, E. (1990). A single amino acid substitution affects multiple overlapping epitopes in the major antigenic site of foot-and-mouth disease virus of serotype C. *J. Gen. Virol.* **71**, 629–637.
16. Curry, S., *et al.*, & Stuart, D. (1992). Crystallisation and preliminary X-ray analysis of three serotypes of foot-and-mouth disease virus. *J. Mol. Biol.* **228**, 1263–1268.
17. Schutt, C. & Winkler, F.K. (1977). The oscillation method for very large unit cells. In *The Rotation Method in Crystallography.* pp. 173–186, North-Holland, Amsterdam.
18. Brünger, A.T. (1992). *X-PLOR Version 3.0.* Yale University, New Haven, CT.
19. Wilson, A.J.C. (1942). Determination of absolute from relative X-ray intensity data. *Nature* **150**, 151–152.
20. Fry, E., Acharya, R. & Stuart, D. (1993). Methods used in the structure determination of foot-and-mouth disease virus. *Acta Crystallogr.A.* **49**, 45–55.
21. Hernández, J., Martínez, M.A., Rocha, E., Domingo, E. & Mateu, M.G. (1992). Generation of a subtype-specific neutralisation epitope in foot-and-mouth disease virus of a different subtype. *J. Gen. Virol.* **73**, 213–216.
22. Palmenberg, A.C. (1989). *Molecular Aspects of Picornavirus Infection and Detection.* American Society for Microbiology, Washington D.C.
23. Krishnaswamy, S. & Rossmann, M.G. (1990). Structural refinement and analysis of mengo virus. *J. Mol. Biol.* **211**, 803–844.
24. Harrison, S.C., Olson, A.J., Schutt, C.E., Winkler, F.K. & Bricogne, G. (1978). Tomato bushy stunt virus at 2.9 Å. *Nature* **276**, 368–373.
25. Silva, A.M. & Rossmann, M.G. (1985). The refinement of southern bean mosaic virus in reciprocal space. *Acta Crystallogr. B.* **41**, 147–157.
26. Chow, M., Newman, J., Filman, D., Hogle, J., Rowlands, D. & Brown, F. (1987). Myristylation of picornavirus capsid protein VP4 and its structural significance. *Nature* **327**, 482–486.
27. Moscufo, N. & Chow, M. (1992). Myristate–protein interactions in poliovirus: interactions of VP4 threonine 28 contribute to the structural conformation of assembly intermediates and the stability of assembled virions. *J. Virol.* **66**, 6849–6857.
28. Fry, E., *et al.*, & Stuart, D. (1990). Architecture and topography of an aphthovirus. *Semin. Virol.* **1**, 439–451.
29. Mateu, M.G., *et al.*, & Domingo, E. (1989). Implications of a quasispecies genome structure: effect on frequent, naturally oc-

curing amino acid substitutions on the antigenicity of foot-and-mouth disease virus. *Proc. Natl. Acad. Sci. USA* **86**, 5883–5887.
30. Mateu, M.G., *et al.*, & Domingo, E. (1987). Reactivity with monoclonal antibodies of viruses from an episode of foot-and-mouth disease virus. *Virus Res.* **8**, 261–274.
31. Parry, N.R., *et al.*, & Lerner, R.A. (1985). Identification of neutralizing epitopes of foot-and-mouth disease virus. In *Vaccines '85*, pp 211–216, Cold Spring Harbour Laboratory, New York.
32. Xie, Q.-C., McCahon, D., Crowther, J.R., Belsham, G.J. & McCullough, K.C. (1987). Neutralisaton of foot-and-mouth disease virus can be mediated through any of at least three separate antigenic sites. *J. Gen. Virol.* **68**, 1637–1647.
33. McCullough, K.C., *et al.*, & McCahon, D. (1986). Epitopes on foot-and-mouth disease virus. *Virology* **157**, 516–525.
34. Martinez, M.A., *et al.*, & Knowles, N.J. (1992). Evolution of the capsid protein genes of foot-and-mouth disease virus particles: antigenic variation without accumulation of amino acid substitutions over six decades. *J. Virol.* **66**, 3557–3565.
35. Mateu, M.G., *et al.*, & Domingo, E. (1994). Antigenic heterogeneity of a foot-and-mouth disease virus in the field is mediated by very limited sequence variation at several antigenic sites. *J. Virol.* **68**, in press.
36. Thomas, A.A.M., Woortmeijer, R.J., Puijk, W. & Barteling, S.J. (1988). Antigenic sites on foot-and-mouth disease virus type A_{10}. *J. Virol.* **62**, 2782–2789.
37. Saiz, J.C., Gonzalez, M.J., Borca, M.V., Sobrino, F. & Moore, D.M. (1991). Identification of neutralising sites on VP1 and VP2 of type A5 foot-and-mouth disease virus, defined by neutralisation resistant variants. *J. Virol.* **65**, 2518–2524.
38. Minor, P.D. (1990). Antigenic structure of picornaviruses. *Curr. Top. in Microbiol. and Immunol.* **161**, 121–154.
39. Wang, G., Porta, C., Chen, Z., Baker, T. & Johnson, J. (1992). Identification of a Fab interaction footprint site on an icosahedral virus by cryoelectron microscopy and X-ray crystallography. *Nature* **355**, 275–278.
40 Kitson, J.D.A., McCahon, D. & Belsham, G.J. (1990). Sequence analysis of monoclonal antibody resistant mutants of type O foot-and-mouth disease virus: evidence for involvement of the three surface exposed capsid proteins in four antigenic sites. *Virology* **179**, 26–34.
41. Novotńy, J., Handschumacher, M. & Bruccoleri, R.E. (1987). Protein antigenicity: a static surface property. *Immunol. Today* **8**, 26–31.
42. Davies, D.R. & Padlan, E.A. (1990). Antibody–antigen complexes. *Annu. Rev. Biochem.* **59**, 439–473.
43. Jin, L., Fendley, B.M. & Wells, J.A. (1992). High resolution functional analysis of antibody–antigen interactions. *J. Mol. Biol.* **226**, 851–865.
44. Acharya, K.R., Ren, J., Stuart, D.I., Phillips, D.C. & Fenna, R.E. (1991). Crystal structure of human α-lactalbumin at 1.7Å resolution. *J. Mol. Biol.* **221**, 571–581.
45. Geysen, H.M., *et al.*, & Lerner, R.A. (1987). Chemistry of antibody binding to a protein. *Science* **235**, 1184–1190.
46. Getzoff, E.D., Tainer, J.A., Lerner, R.A. & Geysen, H.M. (1988). The chemistry and mechanism of antibody binding to protein antigens. *Adv. Immunol.* **43**, 1–98.
47. Westhof, E., *et al.*, & van Regenmortel, M. (1984). Correlation between segmental mobility and the location of antigenic determinants in proteins. *Nature* **311**, 123–126.
48. Strohmaier, K., Franze, R. & Adamm, K.-H. (1982). Location and characterisation of the antigenic portion of the FMDV immunising protein. *J. Gen. Virol.* **59**, 295–306.
49. Bittle, J.L., *et al.*, & Brown, F. (1982). Protection against foot-and-mouth disease by immunisation with a chemically synthesised peptide predicted from the viral nucleotide sequence. *Nature* **298**, 30–33.
50. Pfaff, E., Mussgay, M., Bohm, H.O., Schulz, G.E. & Schaller H. (1982). Antibodies against a preselected peptide recognise and neutralise foot-and-mouth disease virus. *EMBO J.* **1**, 869–874.
51. Domingo, E., Mateu, M.G., Martinez, M.A., Dopazo, J., Moya, A. & Sobrino, F. (1990). Genetic variability and antigenic diversity in foot-and-mouth disease virus. In *Applied Virology Research*, Volume 2, pp 233–266, Plemum Publishing, New York.
52. Mateu, M.G., *et al.*, & Barahona, H. (1988). Extensive antigenic heterogenity of foot-and-mouth disease virus of sterotype C. *Virology* **167**, 113–124.
53. Martínez, M.A., *et al.*, & Mateu, M.G. (1991). Two mechanisms of antigenic diversification of foot-and-mouth disease virus. *Virology* **184**, 695–706.
54. Geysen, H.M., Barteling, S.J. & Meloen, R.H. (1985). Small peptides induce antibodies with a sequence and structural requirement for binding antigen comparable to antibodies raised against the native protein. *Proc. Natl. Acad. Sci. USA* **82**, 178–182.
55. Surovoi, A.Y., Ivanov, V.T., Chepurkin, A.V., Ivanyuschenkov, V.N. & Dryagalin, N.N. (1988). Is the Arg-Gly-Asp sequence the site for foot-and-mouth disease virus binding with cell receptor? *Soviet J. Bioorg. Chem.* **14**, 965–968.
56. Wistow, G., *et al.*, & Blundell, T. (1983). X-ray analysis of the eye lens protein γ-II crystallin at 1.9Å resolution. *J. Mol. Biol.* **170**, 175–202.
57. Leahy, D.J., Hendrickson, W.A., Aukhil, I. & Erickson, H.P. (1992). Structure of a fibronectin type III domain from tenascin phased by MAD analysis of the selenomethionyl protein. *Science* **258**, 987–991.
58. Saudek, V., Atkinson, R.A. & Pelton, J.T. (1991). Three-dimensional structure of echistatin, the smallest active RGD protein. *Biochemistry* **30**, 7369–7372.
59. Adler, M., Lazarus, R.A., Dennis, M.S. & Wagner, G. (1991). Solution structure of kistrin, a potent platelet aggregation inhibitor and GP IIb-IIIa antagonist. *Science* **253**, 445–448.
60. Main, A., Harvey, T., Baron, M., Boyd, J. & Campbell, I. (1992). The three-dimensional structure of the tenth type III module of fibronectin: an insight into RGD-mediated interactions. *Cell* **71**, 671–678.
61. Jones, T.A. (1985). Interactive computer graphics: FRODO. *Meth. Enzymol.* **115**, 157–171.
62. French, S. & Wilson, K. (1978). On the treatment of negative intensity observations. *Acta Crystallogr. A* **34**, 517–525.
63. Jones, T.A., Zou, Y.-J., Cowan, S.W. & Kjeldgaard, M. (1991). Improved methods for building protein models in electron density maps and the location of errors in these models. *Acta Crystallogr. A* **47**, 110–119.
64. Capucci, L., Brocchi, E., De Simone, F. & Panina, G.F. (1984). Characterisation of monoclonal antibodies against foot-and-mouth disease virus. In *Report of a Session of the Research Group of the Standing Technical Committee of the European Commission for the Control of Foot-and Mouth Disease.*, pp 32–39, Food and Agriculture Organisation of the United Nations, Brescia.
65. Wilson, M.B. & Nakane, P.K. (1978). *Immunofluorescence and Related Techniques.* Elsevier, North Holland, Amsterdam.
66. Sobrino, F., *et al.*, & Domingo, E. (1986). Fixation of mutations in the viral genome during an outbreak of foot-and-mouth disease: heterogeneity and rate mutations. *Gene* **50**, 149–159.
67. Fichot, O. & Girard, M. (1990). An improved method for sequencing of RNA templates. *Nucleic Acids Res.* **18**, 6162.
68. Lee, B.K. & Richards, F.M. (1971). The interpretation of protein structures: estimation of static accessibility. *J. Mol. Biol.* **55**, 379–400.
69. Kabsch, W. & Sander, C. (1983). Dictionary of protein secondary structure: pattern recognition of hydrogen-bonded and geometrical features. *Biopolymers* **22**, 2577–2637.

Received: **23 Dec 1993**; revisions requested: **10 Jan 1994**; revisions received: **13 Jan 1994**. Accepted: **14 Jan 1994**.